ELSEVIER



# Novel fluorescent proteins for high-content screening

**Michael Wolff[1], Joerg Wiedenmann[2], G. Ulrich Nienhaus[3,4], Martin Valler[1] and Ralf Heilker[1]**

[1] Department of Lead Discovery, Boehringer Ingelheim Pharma GmbH and Co. KG, Birkendorfer Str.65, D-88397 Biberach, Germany
[2] Department of Zoology and Endocrinology, University of Ulm, D-89069 Ulm, Germany
[3] Department of Biophysics, University of Ulm, D-89069 Ulm, Germany
[4] Department of Physics, University of Illinois at Urbana-Champaign, Urbana, IL 61801, USA

**The development of fast microscopic imaging devices has enabled the application of automated fluorescence microscopy to pharmaceutical high-throughput drug-discovery assays, referred to as high-content screening (HCS). Initially, green fluorescent protein and its derivatives from *Aequorea Victoria*, and later anthozoan fluorescent proteins (FPs) have become potent tools as live-cell markers in HCS assays. We illustrate the broad applicability of classic and novel FPs to drug-discovery assays, giving example applications of the use of FPs in multiplexed imaging as fluorescent timers, photosensitizers and pulse-chase labels, and for robotically integrated compound testing.**

## Fluorescent proteins for high-content screening

Fluorescence microscopy has been employed widely in academic cell biology research as a non-destructive, sensitive technique to visualize subcellular structures and to monitor intracellular protein translocation. In recent years, the pharmaceutical industry has become increasingly interested in studying test compounds in cellular, more disease-relevant assays. In particular, a novel technique that is generally referred to as high-content screening (HCS) has been introduced that combines high-resolution fluorescence microscopy with automated image analysis [1–5].

In HCS, an adherent cell layer at the bottom of a microtitre plate (MTP) well is labelled with several flurorophores and the biomolecules of interest observed by fluorescence microscopy, preferentially in parallel at different wavelengths (multiplexing). Appropriate image-analysis algorithms are employed to quantify the distribution and brightness of the fluorophore-labelled biomolecules in the cells. In live-cell experiments, the kinetics of a drug effect and respective intracellular protein trafficking events can be monitored.

As well as protein trafficking, HCS provides information on the phosphorylation state of target proteins, cellular proliferation and apoptosis, morphological changes such as neurite outgrowth, modifications of the cytoskeleton, cellular movements and other overall changes in fluorescence, such as those observed in the study of gap junctions.

HCS has several benefits compared with standard HTS. Conventional, cellular HTS examines the mean response of the whole cell population in a well. By contrast, HCS resolves discrete responses of individual cells in an MTP well. The individual cells might differ with respect to differentiation, stage of the cell cycle, state of transfection and natural variability. In consequence, heterogeneous effects of a pharmaceutical on mixed-cell populations might be observed in a single MTP well. Therefore, HCS enables the implementation of novel assay formats that do not rely on the overall change of either fluorescence or luminescence intensity from the whole MTP well.

Moreover, HCS provides the chance to correlate 'on-target' drug effects (pharmaceutical effects of a test compound that are related directly to the 'targeted' biomolecule of interest) with other phenomena such as cellular toxicity [6]. Compound artefacts including autofluorescence and cell lysis are discovered readily.

To localize specific biomolecules in a cell using fluorescence microscopy requires that the biomolecules are labelled with an appropriate fluorophore. Classically, molecules have been labelled

*Corresponding author:* Heilker, R. (Ralf.Heilker@bc.boehringer-ingelheim.com)


1359-6446/06/$ - see front matter  doi:10.1016/j.drudis.2006.09.005

by conjugating an organic fluorescent dye (such as fluorescein) to either a ligand or an antibody that recognizes the target structure. However, if the epitope for a ligand or antibody-based fluorescent labelling is not exposed to the extracellular medium, the cells must be fixed and detergent-permeabilized before the fluorescent detection reagent is applied. This fixation procedure restricts cellular imaging to end-point measurements. Alternatively, cDNA that encodes a fluorescent protein (FP) can be cloned into the reading frame of a protein cDNA and expressed by the cell, and the resulting fluorescent fusion protein and its movement kinetics visualized in living cells. In recent years, FPs have been developed into potent tools for fluorescence microscopy. The first FP to be discovered was green FP from the jellyfish *Aequorea victoria* (avGFP) [7–9], which converts the bioluminescent energy generated by a proximal luciferase enzyme by resonance energy transfer into green fluorescence. Several mutants of avGFP have been developed, which display fluorescence emission in the blue to yellow wavelength range [10–12].

Novel, fast, cellular confocal readers such as the Opera™ from Evotec Technologies (Germany), the IN Cell Analyzer 3000™ from General Electrics Healthcare Biosciences (UK) and the BD Pathway Bioimager™ from Becton Dickinson (USA) enable kinetic measurements and real-time monitoring with high spatial and temporal resolution [13]. To exploit the full potential of FP applications in live-cell measurements, some HCS imaging platforms provide incubation chambers that maintain user-defined temperature and carbon dioxide levels [13].

## From GFPs to red FPs as biolabels

The colour range of avGFP-derived mutant proteins has enabled some multiplexing in fluorescence microscopy. However, it was desirable to also cover the red–far-red range of the colour spectrum because the required excitation light for red FPs (RFPs) is less cytotoxic than that for GFPs in fluorometric cellular imaging. Furthermore, there is less interference from light scattering and cytosolic autofluorescence at the higher red-emission wavelengths, and charge-coupled-device cameras that are employed in HCS imaging devices are particularly sensitive to red light.

Initially, the search for alternative FPs focused on bioluminescent organisms such as the sea pens *Renilla* and *Ptilosarcus*. Although FPs have been cloned from these species [14,15], their emission does not extend to wavelengths beyond green. A leap forward to red fluorescence studies in living cells came from the discovery of avGFP homologues in non-bioluminescent anthozoa [16–18]. There is relatively little similarity between anthozoan FPs and avGFP, with around 20% identity at the amino acid sequence level. However, they have a well conserved tertiary structure [19–23], which is referred to as a 'β-can'. The β-can is based on an 11-stranded β-barrel fold, with both barrel openings capped by loop structures. A helix that threads the inner cavity of the β-can contains the chromophore.

For avGFP and the anthozoan FPs, the chromophore is formed by a 4-(p-hydroxybenzylidene)-5-imidazolinone core that is produced by a cyclization and an $O_2$-dependent oxidation reaction involving three subsequent amino acids in the polypeptide chain. The first amino acid of this chromophoric triad is variable: Ser in *Aequorea*, but Gln (DsRed), Met (eqFP611) and His (EosFP, Kaede) in the anthozoan FPs (see below). However, the second (Tyr) and third (Gly) residues are conserved in avGFP and all anthozoan FPs: the Tyr forms the centre of the π-conjugated system and the small side-chain of Gly might be required to overcome spatial restriction. The β-can stabilizes the chromophoric centre via side-chains that protrude into the central cavity and shields the chromophore from quenchers such as molecular oxygen. Both the common principle of the β-can-shielded chromophoric tripeptide and comparative sequence analysis indicate the shared origin of all FPs from a single GFP ancestor [24].

Conveniently, the fluorescence of the anthozoan FPs extends into the red region of the visual spectrum and enables a further level of live-cell multiplexing. The red-shift is brought about by an extension of the chromophore's conjugated π-electron system, which has occurred by convergent evolution (described below) [25]. Some of the initial challenges in applying anthozoan FPs in cellular imaging were the improper protein folding at 37 °C, slow and/or incomplete green-to-red conversion, and formation of dimeric, tetrameric and higher oligomeric structures and aggregates. An unspecific aggregation of the FP probably wrecks the function of the fused protein under study. Also, FP oligomerization forces the resulting fusion protein into non-physiological oligomers that can result in assay artefacts.

## *Discosoma sp.* red fluorescent protein (dsRed): variations on one theme

Most of the above challenges have been addressed by site-directed mutagenesis. DsRed mutagenesis studies [26] first led to a reduction of the 'maturation' time by a factor of 10–15 (where 'maturation' describes the step-wise formation of the FP chromophore; for RFPs this occurs typically via an intermediate green-fluorescent state), and reduced formation of higher-order aggregates. This variant protein, which is available commercially as 'DsRed-Express' (Table 1) lends itself to multiplexing with the optimized avGFP-derivative known as enhanced GFP (EGFP). Particular benefits of the fast maturation of DsRed-Express are evident in rapidly multiplying cells. In an example application, an EGFP-tagged marker for the Golgi complex has been co-expressed with a mitochondrially targeted DsRed-Express in logarithmically growing *Saccharomyces cerevisiae*. Fluorescence microscopy of these fast-growing cells yields bright, cleanly separated, green and red fluorescence signals for the Golgi cisternae and for the mitochondriae, respectively.

Conversely, the slow maturation of another DsRed mutant, DsRed-E5NA (Table 1), its known kinetics of green-to-red conversion and the transient occurrence of a 450 nm emission peak (measured in the blue DAPI channel) can be exploited as an internal fluorescent timer [27]. For example, DsRed-E5NA has been expressed in HEK293 cells under control of the Tet-On inducible system to synchronize and pulse its generation. Figure 1 illustrates how DsRed-E5NA proceeds through various stages of changing fluorescence emission at the three wavelengths monitored, thereby providing a 'timer' function to the respective live-cell experiment. This 'timer' provides an internal time scale that can, for example, measure the kinetics of a pharmaceutical effect.

Additional mutations of the DsRed sequence produced the first anthozoa-derived monomeric FP, called monomeric RFP 1

**TABLE 1**

**Properties of FPs discussed in this review**

| FP | Emission $\lambda_{max}$ (nm) | Applications in HCS-based drug discovery | Refs | Commercially available from |
|---|---|---|---|---|
| DsRed-Express/DsRed.T4 | 586 | Multiplexing with EGFP, avoiding autofluorescence that is typical of medicinal chemistry compounds | [26] | Clontech, Mountain View, CA, USA |
| DsRed-E5NA | 450/500/590 | Fluorescent timer (e.g. for measuring the kinetics of drug effects) | [27] | Clontech, Mountain View, CA, USA |
| mRFP (DsRed-derived) | 607 | Same multiplexing advantages as all above DsRed-derived mutants | [28] | Clontech, Mountain View, CA, USA |
| further mRFP-derived mutants | up to 649 | Broader range of multiplexing options, far-red emission | [29] | cDNAs from PlanetGene, Menlo Park, CA, USA |
| eqFP611/618 | 611/618 | Same multiplexing advantages as all above DsRed-derived mutants, low photobleaching rate | [30,32] | |
| KillerRed | 610 | Chromophore-assisted light inactivation (CALI) of neighbouring proteins (e.g. for target validation) | [37] | Evrogen, Moscow, Russia |
| EosFP | 516/581 | Photoactivatable green-to-red conversion (e.g. for pulse-chase labelling to measure drug-effect kinetics) | [38] | |
| Kaede | 518/580 | Photoactivatable green-to-red conversion like EosFP | [39] | MBL International, Woburn, MA, USA |
| Dendra | 505/575 | Photoactivatable green-to-red conversion like EosFP. Photoconversion can be induced at 488 nm | [41] | Evrogen, Moscow, Russia |
| PS-CFP | 468/511 | Photoactivatable cyan-to-green conversion | [43] | Evrogen, Moscow, Russia |

(mRFP1) (Table 1) [28]. Further mutagenesis of mRFP1 has led to a series of monomeric biolabels (Table 1) with colours that range from green to far-red [29], some of which have an increased fluorescence brightness, a more complete maturation, better tolerance of N-terminal fusions and increased photostability. These optimized DsRed-based FPs fulfil the need for red labels in HCS-based drug discovery that are described earlier.

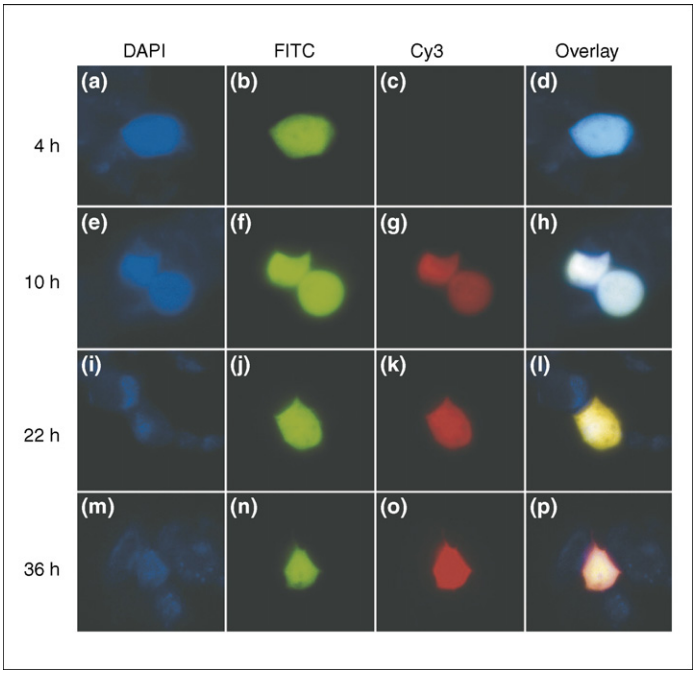


**FIGURE 1**

**Visualization of emission colours of the fluorescent timer DsRed-EFNA in HEK293 cells.** Pulse-chase induction of DsRed-E5NA under the control of the Tet-ON system was used to synchronize expression. **(a–p)** Fluorescence images in the respective wavelength channels (DAPI; a,e,i,m: FITC; b,f,j,n: and Cy3; c,g,k,o) and their overlay (d,h,l,p) show representative, living cells. The overlay images merge the colours of the respective single-colour images. Tet-On induction was performed for 4 h. Images were taken at 4 h (a–d), 10 h (e–h), 22 h (i–l) and 36 h (m–p) after the end of Tet-On induction. Images reprinted with permission from [27].

## eqFP618: application in a G-protein-coupled receptor internalization assay

Discovered in the sea anemone Entacmaea quadricolor, eqFP611 (Table 1) is the most red-shifted natural representative of the FP superfamily (emission maximum at 611 nm) [30]. Similar to DsRed, basic 4-(p-hydroxybenzylidene)-5-imidazolinone core of eqFP611 is extended by an autocatalytic dehydrogenation of the Nα–Cα bond of the first amino acid in the chromophoric triad. Accordingly, DsRed and eqFP611 have almost identical excitation maxima (558 nm and 559 nm, respectively). The chromophores of both DsRed and eqFP611 exist in a coplanar structure in which the hydroxyphenyl group adopts a *cis* configuration in DsRed and a *trans* configuration for eqFP611 [19,22,23,31]. This *trans* configuration and other differences in the chromophore environment might be responsible for the extraordinarily large 52 nm Stokes shift of eqFP611.

Maturation of yellow FPs and RFPs can leave residual amounts of green fluorescent chromophores [27]. Advantageously, in eqFP611, this residual green fluorescence represents <1% of the red fluorescence [30]. Despite the advantages over wild-type DsRed, such as faster, more complete maturation of the red form, the tetrameric nature of eqFP611 has impeded its broader application as a biomarker. However, dimeric mutants of eqFP611 have now been generated [32] that enable the pseudo-monomeric eqFP611 tandem labelling of a target protein. The relatively low photobleaching rate of eqFP611 is an advantage when tracking FP–fusion-proteins in living cells [33]. eqFP618 (Table 1) is an eqFP611-derived mutant with a slightly red-shifted excitation and emission maximum and optimized folding at 37 °C [32]. In an example application, the endothelin A ($ET_A$) receptor has been fused with the pseudo-monomeric tandem construct of eqFP618

and expressed. In stimulated cells, this construct shows that the $ET_A$ receptor localizes to endosomal compartments near the nucleus (data not shown). Internalization assays represent an increasingly popular functional screening format for G-protein-coupled receptors (GPCRs) [34,35]. Fusing a GPCR and red FP, enables GPCR internalization to be monitored in parallel to $Ca^{2+}$-release kinetics, with the latter observed using a $Ca^{2+}$-sensitive green fluorophore.

## KillerRed: a genetically encoded photosensitizer

Chromophore-assisted laser inactivation is a technique whereby a fluorophore is irradiated to produce free reactive oxygen species (ROS), to inactivate a fluorophore-proximal protein. For example, exciting the organic chromophore Malachite green with light at 620 nm produces ROS that cause protein inactivation up to a distance of ~60 Å from the chromophore [36]. In a biological application of this principle, the fluorophore might be conjugated to a biological entity close to the target protein for photoinactivation. One potential obstacle to applying this technique in cell biology is that the chromophore must be brought to the location of intended photodestruction, possibly across the cell membrane. To address this challenge, an FP-based photosensitizer with an excitation maximum at 585 nm, referred to as KillerRed (Table 1), has been developed by mutagenesis of the hydrozoan chromoprotein anm2CP [37].

In an example application, EGFP, the pleckstrin homology (PH) domain of phospholipase Cδ1 and KillerRed have been expressed as a triple-fusion protein (Figure 2). On irradiation with green light, KillerRed generates ROS and destroys the function of the conjugated PH domain. Such an inducible protein knockout in a live-cell experiment might be a valuable drug-discovery tool, for example in HCS-based validation of a drug target.

## EosFP: a 'pulse-chase' label

Some photoctivatable FPs feature a light-induced green-to-red photoconversion. This property is especially convenient for microscopy applications because the structures highlighted are identified readily by their initial green fluorescence. EosFP (Table 1), which was cloned originally from the stony coral *Lobophyllia hemprichii* [38], is such a photoconverting FP. X-ray analysis of EosFP crystals [20] show that the molecular structure of each EosFP subunit has the same β-can fold as avGFP. Similar to the anthozoa-derived Kaede (Table 1) [39], it irreversibly changes its fluorescence emission maximum from 516 nm to 581 nm on irradiation with ~350–440 nm light. This shift of the emission spectrum is associated with photolysis of the polypeptide backbone between the Nα and Cα

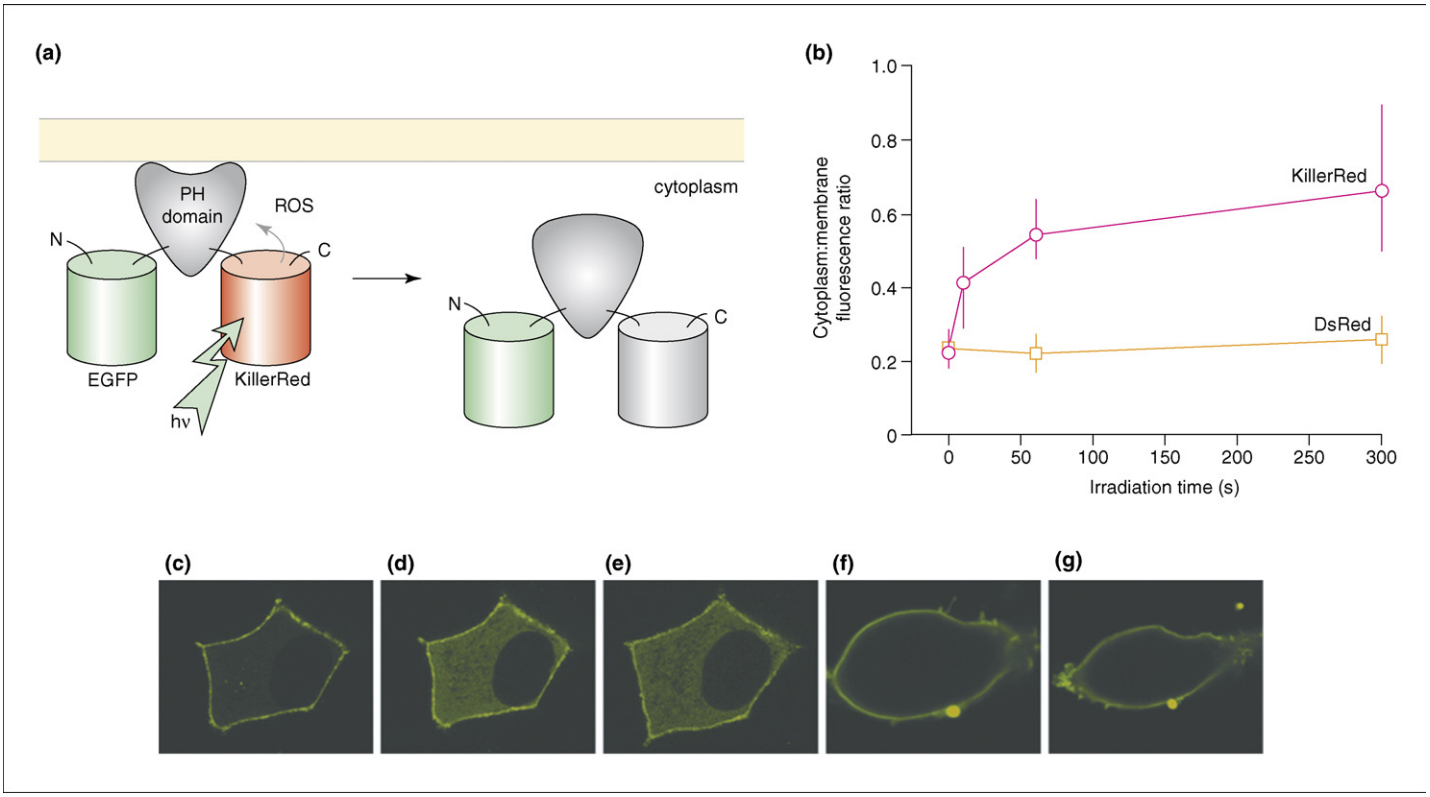


**FIGURE 2**

**Schematic of the experimental system (a).** Normally, the EGFP–PH–KillerRed triple-fusion protein is localized predominantly at the plasma membrane because of the specific affinity of the PH domain for the membrane lipid PtdIns (4,5)$P_2$. Irradiation with intense green light leads to the generation of ROS by KillerRed and damage to the adjacent PH domain, which causes the fusion protein to dissociate from the membrane. **(b)** Dependence of EGFP–PH–KillerRed (magenta circles) and EGFP–PH–DsRedExpress (red squares) membrane-to-cytoplasm translocation on the irradiation time. **(c,d,e)** Confocal images of a cell expressing EGFP–PH–KillerRed triple fusion (EGFP green fluorescent signal) before (c), after (d) and 1.5 h after (e) 10-s irradiation with green light. Note the increase in cytoplasmic signal in (d,e). **(f,g)** Control experiment showing a cell expressing the EGFP–PH–DsRedExpress triple fusion (EGFP green fluorescent signal) before (f) and after (g) 1-min irradiation with green light. No change in signal distribution within the cell was observed. Images reprinted with permission from [37].

atoms of the His in the first position of the chromophore tripeptide both for EosFP and for Kaede [20,40]. More recently, another photoconvertable FP has been described, Dendra (Table 1) [41], that can be converted conveniently using a 488 nm laser.

Wild-type EosFP displays a 'dimer of dimers' subunit arrangement [20], which is characteristic of anthozoan FPs [23]. Folding of monomeric EosFP mutants and, thus, cellular studies are so far restricted to temperatures <30 °C. Substitution of Thr158 by either His or Arg disrupts one of the tetrameric interfaces and results in dimeric variants that fold correctly at 37 °C. Therefore, a tandem of two EosFP (T158R) mutant subunits (t2EosFP) connected by a 12-amino-acid linker has been employed in cell-biological studies. In a variation of this theme, a second tandem construct has been produced (t1EosFP) that contains the chromophore-extinguishing Tyr63Gly mutation in the first of the two EosFP subunits, leaving only the second copy of EosFP with a functional chromophore [42]. These EosFP tandems have enabled the fusion-protein labelling of the androgen receptor (AR) and the $ET_A$ receptor, and the study of these fusion proteins in a cellular environment at 37 °C. The applicability to pulse-chase experiments has been demonstrated using an AR–t1EosFP fusion protein (Figure 3). The cyan-to-green photoconversion of photoswitchable cyan fluorescent protein (PS-CFP) (Table 1) can potentially be exploited in a similar manner [43].

In drug-discovery-directed HCS assays, such pulse-chase labels are particularly helpful for long-term (i.e. lasting several hours) measurements of test compounds that distinguish the effects of a compound on the photoconverted FP fusion protein from those on the unconverted, newly synthesized, FP fusion protein.

## FP labels for robotically integrated, fast-kinetics HCS

Abolishing the need for multistep, post-fixation, immunostaining procedures, the endogenously formed chromophores of FPs lend themselves excellently to automated HCS testing. In an example application, a robotically integrated HCS assay was established to investigate the effects of test compounds on the phosphatidylinositol 3-kinase (PI 3-kinase)/AKT1 signalling pathway [6] by stably transfecting CHO cells with both human insulin receptor (hIR) and human homologue 1 of the AKR mouse Thymoma-derived viral oncogene (AKT1)–EGFP. Stimulation of hIR with insulin-like growth factor-1 (IGF-1) induced the partial translocation of cytosolic AKT1-EGFP to specific regions of the plasma membrane, where phosphatitylinositol (3,4,5)-trisphosphate

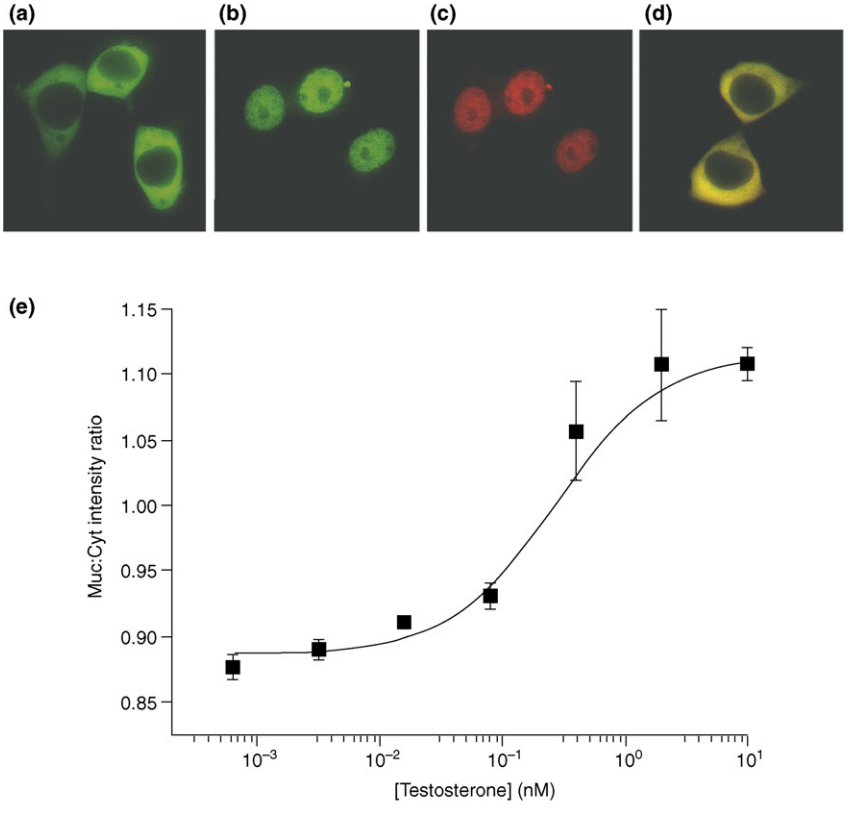


**FIGURE 3**

**Translocation of the AR. (a)** Cytoplasmic localization of the AR–t1EosFP fusion protein before stimulation with testosterone in HEK293 cells. Scale bar, 20 μm (representative of images a–d). **(b)** AR–t1EosFP translocates to the nucleus on stimulation with testosterone. **(c)** Photoconversion of nuclear protein enables red labelling of translocated protein and **(d)** back-transport to the cytoplasm caused by removing the hormone. The yellow colour indicates that both newly expressed GFP and converted protein are in the cytoplasm. **(e)** Dose–response curve for testosterone measured using the image-analysis software of the IN Cell Analyzer 3000™ (General Electric Healthcare Biosciences, UK) for nuclear translocation. Reprinted with permission from [42].

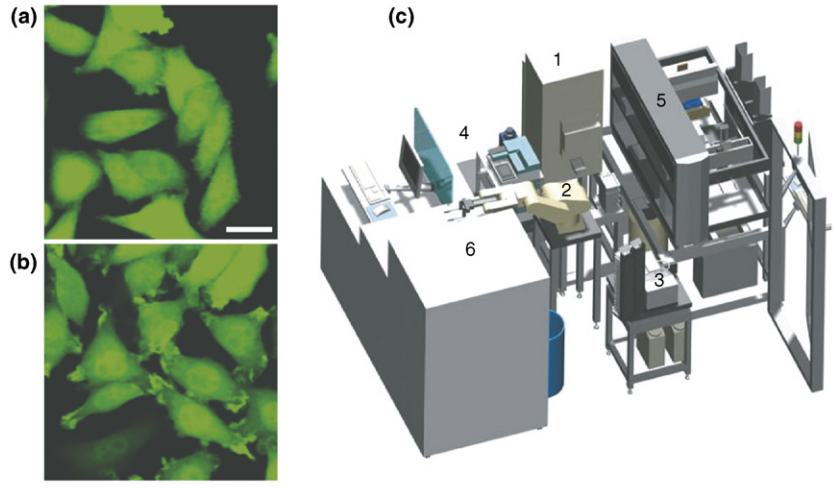


**FIGURE 4**

**Robotically integrated AKT1–EGFP translocation assay.** CHO cells expressing an AKT1–EGFP fusion construct were stimulated with IGF-1. **(a)** In non-stimulated cells AKT1–EGFP occurs throughout the cells. Scale bar, 20 μm (representative of images a and b). **(b)** AKT1–EGFP translocation in IGF-1-stimulated cells is visible as bright fluorescent spots at the plasma membrane. **(c)** Integration of AKT1–EGFP translocation assay into a robotic environment. Assay MTPs with adherent cell layers are loaded to the Cytomat 2 C15™ (Thermo Electron Corp., USA; 1). The CRS F3 robotic arm (Thermo Electron Corp., USA; 2) transfers an MTP first to the BioTek™ MTP Washer (BioTek Instruments Inc., USA; 3) then to one of three Multidrop dispensers (Thermo Electron Corp., USA; 4) for addition of assay buffer. The MTP is transported to the Freedom EVO™ liquid handling workstation (Tecan, Switzerland; 5), for test-compound transfer. Agonist is added (4) and, after another incubation (1), fixation and/or nuclear stain solution is added. Translocation of AKT1–EGFP is measured in the IN Cell Analyzer 3000™ (6).

[PtdIns-(3,4,5)$P_3$] and PtdIns-(3,4)$P_2$ are enriched in lipid rafts (Figure 4a,b). A robotically integrated end-point assay was established (Figure 4c), and automated HCS used to identify compounds that inhibit PI 3-kinaseα and, thereby, hinder translocation of AKT1–EGFP to the plasma membrane. Automated dose-response testing displayed excellent reproducibility, and background staining of the cytosol by EGFP enabled additional detection of cytotoxic side-effects of the compounds, based on a cellular rounding.

## Impact of the new fluorescent proteins on HCS-based drug discovery

At the time of their discovery, many anthozoan FPs in their wild-type forms were suited poorly for application in pharmaceutical compound testing because of their slow maturation, oligomerization and/or aggregation, low fluorescence intensity and improper folding at 37 °C. As described above, most of these challenges have been overcome by a combination of directed and random mutagenesis.

Several anthozoan FPs have emission spectra that extend into the red region of the visual spectrum. In the context of drug-discovery assays, this enables the FP fluorescence to be detected in the presence of autofluorescent test compounds that, typically, have shorter wavelength emission. Furthermore, pharmaceutical compound testing often aims to cover both the direct effects and the side-effects on a target cell in a single assay. In fluorometric, live-cell imaging, this requires the parallel application of differently coloured fluorophore labels, such as the classic GFPs and the novel RFPs. For multicolour imaging, it is important that both FP labels generate their chromophoric centres with a similar velocity. Recently, protein engineering has yielded RFPs with similar maturation kinetics to avGFP, which makes them suited for multiplexing with avGFP.

Another important feature of drug discovery is to measure the cellular response kinetics of a pharmaceutical test compound. To address this need, a 'fluorescent timer' protein such as DsRed-E5NA might be employed in a live-cell experiment as a kinetic reporter protein for a drug effect. Similarly, pulse-chase FP labels on a target protein enable the kinetic investigation of the effects of a test compound over several hours by distinguishing the cellular distribution of the photoconverted FP–target conjugate from non-photoconverted, newly synthesized, FP–target proteins.

Last, as illustrated above, FP biolabels support automated drug testing because they do not require cumbersome immune-staining procedures such as cell permeabilization, primary and/or secondary antibody-incubation and supernatant-washing steps.

## Conclusions and outlook

In this review, we describe a series of novel FPs and their possible applications in HCS. These tools complement existing HCS tools that are based on avGFP-derived biolabels, which have been reviewed previously [44]. In addition to the specific examples described above, novel FPs might be employed similarly to the avGFP-derived mutants, for example in fluorescence resonance energy transfer (FRET) pairs to detect either intracellular $Ca^{2+}$ [45,46] or $Cl^-$ concentrations [47], and to measure protein phosphorylation [48], protein–protein interactions [49] and protein cleavage [50]. The unique property of FPs to act as endogenously expressed biolabels for fluorescence microscopy makes them particularly attractive for use in HCS-type, live-cell, drug-discovery assays. The red fluorescence of the novel FPs adds the benefit of reduced interference from cellular autofluorescence and from the

typical fluorescence wavelength spectrum of several medicinal chemistry compounds. Thus, the new FPs incorporate technologically useful features that enable the design of sophisticated, novel assay formats for drug discovery.

## References


1 Ghosh, R.N. *et al.* (2000) Cell-based, high-content screen for receptor internalization, recycling and intracellular trafficking. *Biotechniques* 29, 170–175
2 Almholt, D.L. *et al.* (2004) Nuclear export inhibitors and kinase inhibitors identified using a MAPK-activated protein kinase 2 redistribution screen. *Assay Drug Dev. Technol.* 2, 7–20
3 Li, Z. *et al.* (2003) Identification of gap junction blockers using automated fluorescence microscopy imaging. *J. Biomol. Screen.* 8, 489–499
4 Conway, B.R. *et al.* (1999) Quantification of G-Protein coupled receptor internatilization using G-Protein coupled receptor-green fluorescent protein conjugates with the arrayscantrade mark high-content screening system. *J. Biomol. Screen.* 4, 75–86
5 Taylor, D.L. *et al.* (2001) Real-time molecular and cellular analysis: the new frontier of drug discovery. *Curr. Opin. Biotechnol.* 12, 75–81
6 Wolff, M. *et al.* (2006) Automated High Content Screening for phosphoinositide 3 kinase inhibition using an AKT1 redistribution assay. *Comb. Chem. High Throughput Screen.* 9, 339–350
7 Shimomura, O. *et al.* (1962) Extraction, purification and properties of aequorin, a bioluminescent protein from the luminous hydromedusan, Aequorea. *J. Cell. Comp. Physiol.* 59, 223–239
8 Prasher, D.C. *et al.* (1992) Primary structure of the Aequorea victoria green-fluorescent protein. *Gene* 111, 229–233
9 Chalfie, M. *et al.* (1994) Green fluorescent protein as a marker for gene expression. *Science* 263, 802–805
10 Heim, R. *et al.* (1994) Wavelength mutations and posttranslational autoxidation of green fluorescent protein. *Proc. Natl. Acad. Sci. U. S. A.* 91, 12501–12504
11 Heim, R. and Tsien, R.Y. (1996) Engineering green fluorescent protein for improved brightness, longer wavelengths and fluorescence resonance energy transfer. *Curr. Biol.* 6, 178–182
12 Tsien, R.Y. (1998) The green fluorescent protein. *Annu. Rev. Biochem.* 67, 509–544
13 Zemanova, L. *et al.* (2003) Confocal optics microscopy for biochemical and cellular high-throughput screening. *Drug Discov. Today* 8, 1085–1093
14 Peelle, B. *et al.* (2001) Characterization and use of green fluorescent proteins from Renilla mulleri and Ptilosarcus guernyi for the human cell display of functional peptides. *J. Protein Chem.* 20, 507–519
15 Chalfie, M. (1995) Green fluorescent protein. *Photochem. Photobiol.* 62, 651–656
16 Matz, M.V. *et al.* (1999) Fluorescent proteins from nonbioluminescent Anthozoa species. *Nat. Biotechnol.* 17, 969–973
17 Wiedenmann, J. (1997) Die Anwendung eines orange fluoreszierenden Proteins und weiterer Proteine und der zugehörenden Gene aus der Artengruppe Anemonia sp. (sulcata) Pennant, (Cnidaria, Anthozoa, Actinaria) in Gentechnologie und Molekularbiologie, DE 197 18 640 A1 DPMA ed., pp 1–18.
18 Wiedenmann, J. *et al.* (2000) Cracks in the beta-can: fluorescent proteins from Anemonia sulcata (Anthozoa, Actinaria). *Proc. Natl. Acad. Sci. U. S. A.* 97, 14091–14096
19 Nienhaus, K. *et al.* (2003) Crystallization and preliminary X-ray diffraction analysis of the red fluorescent protein eqFP611. *Acta Crystallogr. D Biol. Crystallogr.* 59, 1253–1255
20 Nienhaus, K. *et al.* (2005) Structural basis for photo-induced protein cleavage and green-to-red conversion of fluorescent protein EosFP. *Proc. Natl. Acad. Sci. U. S. A.* 102, 9156–9159
21 Ormo, M. *et al.* (1996) Crystal structure of the Aequorea victoria green fluorescent protein. *Science* 273, 1392–1395
22 Petersen, J. *et al.* (2003) The 2.0-A crystal structure of eqFP611, a far red fluorescent protein from the sea anemone Entacmaea quadricolor. *J. Biol. Chem.* 278, 44626–44631
23 Wall, M.A. *et al.* (2000) The structural basis for red fluorescence in the tetrameric GFP homolog DsRed. *Nat. Struct. Biol.* 7, 1133–1138
24 Shagin, D.A. *et al.* (2004) GFP-like proteins as ubiquitous metazoan superfamily: evolution of functional features and structural complexity. *Mol. Biol. Evol.* 21, 841–850
25 Ugalde, J.A. *et al.* (2004) Evolution of coral pigments recreated. *Science* 305, 1433
26 Bevis, B.J. and Glick, B.S. (2002) Rapidly maturing variants of the discosoma red fluorescent protein (DsRed). *Nat. Biotechnol.* 20, 83–87
27 Verkhusha, V.V. *et al.* (2004) Common pathway for the red chromophore formation in fluorescent proteins and chromoproteins. *Chem. Biol.* 11, 845–854
28 Campbell, R.E. *et al.* (2002) A monomeric red fluorescent protein. *Proc. Natl. Acad. Sci. U. S. A.* 99, 7877–7882
29 Wang, L. *et al.* (2004) Evolution of new nonantibody proteins via iterative somatic hypermutation. *Proc. Natl. Acad. Sci. U. S. A.* 101, 16745–16749
30 Wiedenmann, J. *et al.* (2002) A far-red fluorescent protein with fast maturation and reduced oligomerization tendency from Entacmaea quadricolor (Anthozoa, Actinaria). *Proc. Natl. Acad. Sci. U. S. A.* 99, 11646–11651
31 Gross, L.A. *et al.* (2000) The structure of the chromophore within DsRed, a red fluorescent protein from coral. *Proc. Natl. Acad. Sci. U. S. A.* 97, 11990–11995
32 Wiedenmann, J. *et al.* (2005) Red fluorescent protein eqFP611 and its genetically engineered dimeric variants. *J. Biomed. Opt.* 10, 14003
33 Steinmeyer, R. *et al.* (2005) Improved fluorescent proteins for single-molecule research in molecular tracking and co-localization. *J. Fluoresc.* 15, 707–721
34 Milligan, G. (2003) High-content assays for ligand regulation of G-protein-coupled receptors. *Drug Discov. Today* 8, 579–585
35 Haasen, D. *et al.* (2006) G protein-coupled receptor internalization assays in the High Content Screening format. *Methods in Enzymology* 414, 121–139
36 Linden, K.G. *et al.* (1992) Spatial specificity of chromophore assisted laser inactivation of protein function. *Biophys. J.* 61, 956–962
37 Bulina, M.E. *et al.* (2006) A genetically encoded photosensitizer. *Nat. Biotechnol.* 24, 95–99
38 Wiedenmann, J. *et al.* (2004) EosFP, a fluorescent marker protein with UV-inducible green-to-red fluorescence conversion. *Proc. Natl. Acad. Sci. U. S. A.* 101, 15905–15910
39 Ando, R. *et al.* (2002) An optical marker based on the UV-induced green-to-red photoconversion of a fluorescent protein. *Proc. Natl. Acad. Sci. U. S. A.* 99, 12651–12656
40 Mizuno, H. *et al.* (2003) Photo-induced peptide cleavage in the green-to-red conversion of a fluorescent protein. *Mol. Cell* 12, 1051–1058
41 Gurskaya, N.G. *et al.* (2006) Engineering of a monomeric green-to-red photoactivatable fluorescent protein induced by blue light. *Nat. Biotechnol.* 24, 461–465
42 Nienhaus, G.U. *et al.* (2005) Photoconvertible fluorescent protein eosfp-biophysical properties and cell biology Applications. *Photochem. Photobiol.* 82, 351–358
43 Chudakov, D.M. *et al.* (2004) Photoswitchable cyan fluorescent protein for protein tracking. *Nat. Biotechnol.* 22, 1435–1439
44 van Roessel, P. and Brand, A.H. (2002) Imaging into the future: visualizing gene expression and protein interactions with fluorescent proteins. *Nat. Cell Biol.* 4, E15–E20
45 Miyawaki, A. *et al.* (1997) Fluorescent indicators for Ca2+ based on green fluorescent proteins and calmodulin. *Nature* 388, 882–887
46 Miyawaki, A. *et al.* (1999) Dynamic and quantitative Ca2+ measurements using improved cameleons. *Proc. Natl. Acad. Sci. U. S. A.* 96, 2135–2140
47 Kuner, T. and Augustine, G.J. (2000) A genetically encoded ratiometric indicator for chloride: capturing chloride transients in cultured hippocampal neurons. *Neuron* 27, 447–459
48 Nagai, Y. *et al.* (2000) A fluorescent indicator for visualizing cAMP-induced phosphorylation *in vivo*. *Nat. Biotechnol.* 18, 313–316
49 Mochizuki, N. *et al.* (2001) Spatio-temporal images of growth-factor-induced activation of Ras and Rap1. *Nature* 411, 1065–1068
50 Xu, X. *et al.* (1998) Detection of programmed cell death using fluorescence energy transfer. *Nucleic Acids Res.* 26, 2034–2035